CrossMark

JWST/MIRI Spectroscopy of the Disk of the Young Eruptive Star EX Lup in Quiescence

Ágnes Kóspál[1,2,3,4] ⓘ, Péter Ábrahám[1,2,4] ⓘ, Lindsey Diehl[5], Andrea Banzatti[5] ⓘ, Jeroen Bouwman[3] ⓘ, Lei Chen[1,2] ⓘ,
Fernando Cruz-Sáenz de Miera[1,2] ⓘ, Joel D. Green[6,7] ⓘ, Thomas Henning[3] ⓘ, and Christian Rab[8,9] ⓘ

[1] Konkoly Observatory, Research Centre for Astronomy and Earth Sciences, Eötvös Loránd Research Network (ELKH), Konkoly-Thege Miklós út 15-17, 1121
Budapest, Hungary; kospal.agnes@csfk.org
[2] CSFK, MTA Centre of Excellence, Konkoly-Thege Miklós út 15-17, 1121 Budapest, Hungary
[3] Max Planck Institute for Astronomy, Königstuhl 17, D-69117 Heidelberg, Germany
[4] ELTE Eötvös Loránd University, Institute of Physics, Pázmány Péter sétány 1/A, 1117 Budapest, Hungary
[5] Department of Physics, Texas State University, 749 N Comanche Street, San Marcos, TX 78666, USA
[6] The University of Texas at Austin, Department of Astronomy, 2515 Speedway, Stop C1400, Austin, TX 78712, USA
[7] Space Telescope Science Institute, 3700 San Martin Drive, Baltimore, MD 02138, USA
[8] University Observatory, Faculty of Physics, Ludwig-Maximilians-Universität München, Scheinerstr. 1, D-81679, Munich, Germany
[9] Max-Planck-Institut für Extraterrestrische Physik, Giessenbachstr. 1, D-85748, Garching, Germany
Received 2022 December 16; revised 2023 January 19; accepted 2023 January 19; published 2023 March 1

Abstract

EX Lup is a low-mass pre-main-sequence star that occasionally shows accretion-related outbursts. Here, we present
JWST/MIRI medium-resolution spectroscopy obtained for EX Lup 14 yr after its powerful outburst. EX Lup is
now in quiescence and displays a Class II spectrum. We detect a forest of emission lines from molecules previously
identified in infrared spectra of classical T Tauri disks: H_2O, OH, H_2, HCN, C_2H_2, and CO_2. The detection of
organic molecules demonstrates that they are back after disappearing during the large outburst. Spectral lines from
water and OH are for the first time deblended and will provide a much-improved characterization of their
distribution and density in the inner disk. The spectrum also shows broad emission bands from warm, submicron-
size amorphous silicate grains at 10 and 18 μm. During the outburst, in 2008, crystalline forsterite grains were
annealed in the inner disk within 1 au, but their spectral signatures in the 10 μm silicate band later disappeared.
With JWST we rediscovered these crystals via their 19.0, 20.0, and 23.5 μm emission, the strength of which
implies that the particles are at ∼3 au from the star. This suggests that crystalline grains formed in 2008 were
transported outwards and now approach the water snowline, where they may be incorporated into planetesimals.
Containing several key tracers of planetesimal and planet formation, EX Lup is an ideal laboratory to study the
effects of variable luminosity on the planet-forming material and may provide an explanation for the observed high
crystalline fraction in solar system comets.

Unified Astronomy Thesaurus concepts: Protoplanetary disks (1300); Eruptive variable stars (476); Low mass stars
(2050); Infrared spectroscopy (2285)

Supporting material: data behind figure

1. Introduction

Circumstellar disks provide the material that forms stars and
planetary systems. Dust grains in the disk make rocky planets
and the cores of gas giants, while the forming planets may
accrete their atmospheres directly from the disk's gas content or
when the grains' ice mantles sublimate. Therefore, studying the
composition of protoplanetary disks is needed to understand
the initial mineralogical and chemical composition that the
young planets inherit (e.g., Jørgensen et al. 2020; Eistrup &
Henning 2022; Wordsworth & Kreidberg 2022).

Infrared spectroscopy is an excellent tool to investigate the
warm material in protoplanetary disks. The small, amorphous
silicate grains that the disks of T Tauri stars inherit from the
interstellar medium have prominent broad features around
9.7 μm due to the SiO stretching modes and around 18 μm due
to OSiO bending modes (Henning 2010). During their
evolution, these silicates may undergo thermal processing and
form crystalline silicates such as forsterite and enstatite, which
have multiple narrow features at infrared wavelengths (e.g.,

Fabian et al. 2001). The infrared regime is rich in rotational and
rovibrational lines of gas-phase molecules and broad bands of
molecular ices. These have been extensively studied using
space missions like the Infrared Space Observatory (e.g., van
Dishoeck 2004, and references therein), the Spitzer Space
Telescope (e.g., Boogert et al. 2008; Pontoppidan et al. 2010),
the Herschel Space Observatory (e.g., Dent et al. 2013; Fedele
et al. 2013), and now the JWST.

While circumstellar disks typically evolve on 10^5–10^6 yr
timescales (Williams & Cieza 2011), variable heating and
changing irradiation during accretion bursts and outbursts may
change them significantly faster (Fischer et al. 2022). Due to
the released energy, outbursts can have significant effects on
the disk material, modifying its physical, chemical, and
mineralogical properties (Molyarova et al. 2018; Ábrahám
et al. 2019). As eruptions overlap with the earliest stages of
planet formation, episodic accretion may have far-reaching
consequences for disk evolution and planet formation (e.g.,
Cieza et al. 2016).

The best-studied example of accretion outburst-induced
changes is EX Lup, the prototype of the EXor class of young
eruptive stars (Herbig 1989). In 2008, EX Lup exhibited its
largest outburst ever observed ($\Delta V \sim 5$mag). A multiwave-
length, multiepoch investigation of this event revealed the

annealing of amorphous silicates to crystalline grains, detected via their 10 and 11.3 μm emission (Ábrahám et al. 2009). In parallel, Banzatti et al. (2012, 2015) reported increased strength for OH and H_2O lines during the outburst, while organics, such as C_2H_2 and HCN, disappeared, possibly due to UV photodissociation.

In the course of the year following the outburst, the spectral signatures of the crystalline grains at 10 and 11.3 μm gradually weakened and later disappeared (Ábrahám et al. 2019). During the 2008 outburst, cold forsterite emission also appeared between 15 and 35 μm, which became even stronger after the end of the outburst in late 2008 to early 2009. As these long-wavelength features were not present before the outburst, Juhász et al. (2012) proposed that the crystals formed in the inner disk and were transported to outer disk regions driven by a low-velocity wind. Based on this idea, Ábrahám et al. (2019) performed radiative transfer modeling of multiepoch mid-infrared spectra. They predicted that the crystalline grains cooled down and are now located $\geqslant 3$ au from the central star, but could be as far as $\sim$10 au (with an expansion velocity of $\sim$3 km s^{-1}). If the forsterite grains can reach the water snowline at 3.5 au on the disk surface (Ábrahám et al. 2009), they may bring crystalline material to newly forming planetesimals and reveal the details of the radial transport processes in the disk. After Spitzer but before JWST, we lacked the sensitivity and wavelength coverage to detect these cold crystals.

Apart from smaller bursts in 2011 and early 2022 (Ábrahám et al. 2019; Kóspál et al. 2022; Zhou & Herczeg 2022), EX Lup has been in quiescence since 2008. While it may currently be similar to a typical, quiescent T Tauri disk, it also offers an opportunity to study possible residual effects from the 2008 large outburst. To survey the mid-infrared spectral features in EX Lup's disk, we observed it with the medium-resolution spectrometer (MRS) of JWST's Mid-Infrared Instrument (MIRI). Here, we present our first results based on this spectrum.

2. Observations and Data Reduction

We obtained JWST/MIRI MRS spectroscopy of EX Lup on 2022 August 23 (GO 2209, PI: P. Ábrahám). We used all four channels and all three sub-bands, covering 4.9–28 μm at a spectral resolution of 3500–1500. We observed a separate background 193$''$5 away from EX Lup, centered at R.A.$_{\mathrm{J2000}} = 16^h03^m12^s63$, decl.$_{\mathrm{J2000}} = -40°15'30''42$. Exposure time was 344.1 s for the science target and 41.6 s for the background. We used the FASTR1 readout mode and four-point dithering for EX Lup and no dithering for the background. We reduced the spectra by running the JWST pipeline version 1.8.2. Dedicated background exposures were subtracted from the exposure level products to remove the thermal background. We further applied a residual fringe correction based on the empirical sine model fitting method described in, e.g., Kester et al. (2003) and P. J. Kavanagh et al. 2023 (in preparation). The correction fits and removes fringe residuals that are assumed to be low in amplitude after the application of the fringe flat correction in the pipeline.

The spacecraft pointing information was about 1$''$2 offset from the actual pointing inferred from both the MIRI integral field data and MIRI simultaneous images. Due to this, EX Lup was not well centered in the MRS field of view; a significant part of the source was cut off in two of the four dither positions

observed in the short-wavelength channels, where the field of view was the smallest. We discarded the affected dithers when constructing the spectral cubes for channels 1 and 2.

To check whether JWST spatially resolved the mid-infrared emission of EX Lup, we compared the 3D data cubes with similar measurements of a point-source template. We used 10 Lac, observed within the calibration program 1524 (PI: D. R. Law) with the purpose of characterizing the point-spread function of MIRI MRS. After rotating, shifting, scaling, and subtracting the 10 Lac measurements from the EX Lup measurements channel by channel, we found that the residuals were typically below a few percent. A comparison between 2D Gaussian sizes fitted to EX Lup and 10 Lac did not reveal any significant difference in the 4.9–26.5 μm range. At longer wavelengths, 10 Lac was too faint to be detected reliably. Thus, EX Lup remained unresolved by MIRI.

We calculated the centroid for each image in the 3D data cube and used aperture photometry to extract the 1D spectrum using the default parameters for point sources. Flux levels of different channels and sub-bands (for the usable dither positions) were in general consistent within 5% in the overlapping wavelength ranges. One exception is the channel 4 medium sub-band (20.8–24.3 μm), which was lower by 10%. We corrected these mismatches by applying multiplicative factors determined in the overlapping regions. No scaling was applied to channel 2 (7.6–11.7 μm). The observed shifts between the spectral channels are consistent with the quoted 10% absolute flux calibration uncertainty determined during the commissioning of the MRS instrument.[10] To the best of our knowledge, the only remaining instrumental artifact is the dip around 12.25 μm due to a spectral leak.

To check the accuracy of the wavelength calibration of our spectrum, we measured the wavelengths of 139 strong nonblended water emission lines (Section 3) and computed the shifts compared to the theoretical wavelengths. According to the documentation, the wavelength calibration of MIRI MRS is accurate to within 1 spectral resolution element (85–200 km s^{-1} depending on channel and sub-band). We found that the measured shifts are less than 0.0015 μm below 10 μm and less than 0.003 μm above 10 μm, much better than the nominal accuracy.

The final spectrum is plotted in Figure 1. As representative values, we reached signal-to-noise ratios (S/Ns) of 120 at 9.0 μm, 100 at 15.5 μm, and 60 at 25.0 μm on the continuum.

3. Results and Analyses

3.1. Spectral Energy Distribution

The MIRI MRS spectrum of EX Lup, plotted in F_ν, slowly rises toward longer wavelengths between 4.9 and 8 μm, after which a prominent 10 μm silicate emission feature is visible. Above 13 μm, the spectrum increases again until $\sim$18 μm, where a shallow, broad 18 μm silicate feature begins. Apart from some weaker, narrower silicate features between 18 and 24 μm, the spectrum is approximately flat here, then slowly decreases toward longer wavelengths.

At the date of the MIRI observation (2022 August), EX Lup was in quiescence following a medium-sized burst occurring between 2022 February–April (F. Cruz-Sáenz de Miera et al. 2023, in preparation). Thus, we compared the spectral shape

---

[10] https://www.stsci.edu/files/live/sites/www/files/home/jwst/documentation/_documents/jwst-science-performance-report.pdf
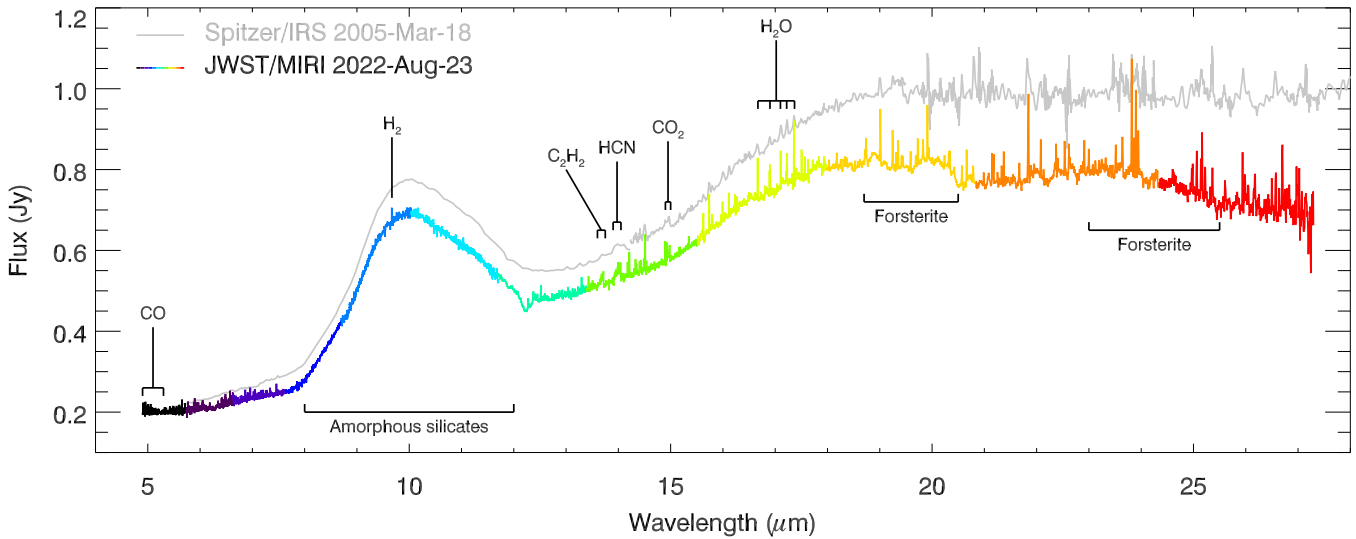
Figure 1. JWST/MIRI MRS spectrum of EX Lup (color), shown together with an earlier Spitzer/IRS spectrum (gray), both taken in quiescence. The different colors mark the individual sub-bands of the JWST spectrum. We indicated some of the observed molecular and solid-state features. We note that the spectrum contains hundreds of H_2O lines; we only marked a few of them as an illustration.
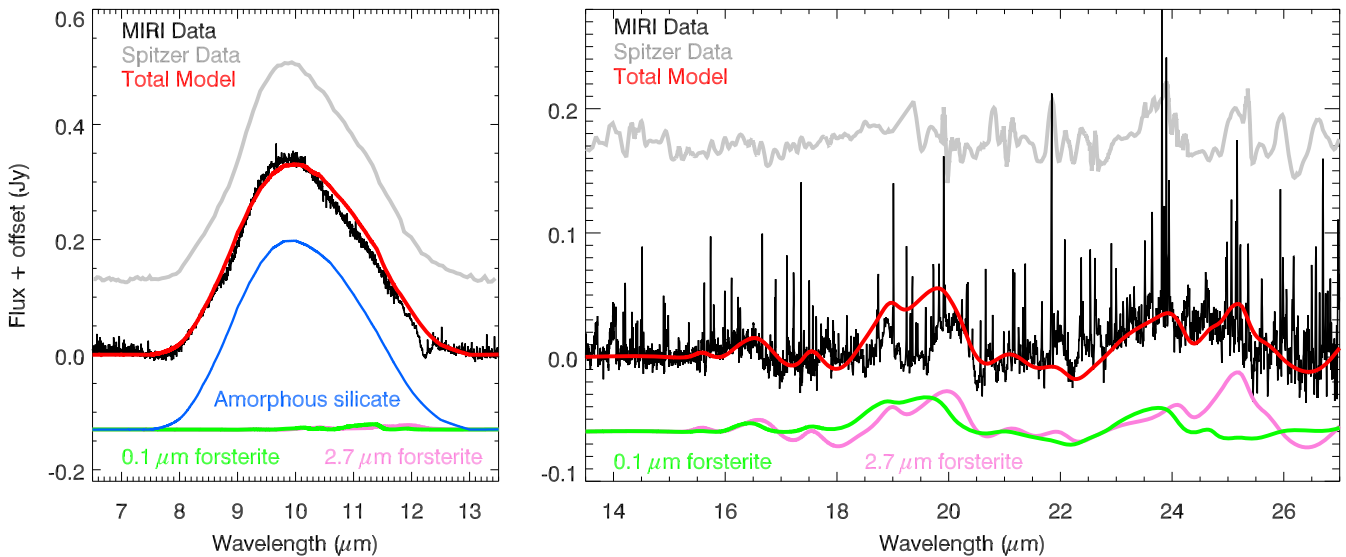
(The data used to create this figure are available.)

Figure 2. Continuum-subtracted JWST/MIRI spectrum of EX Lup with various dust models and with the Spitzer/IRS quiescent spectrum from 2005. The model curves were shifted for clarity.

with an earlier quiescent spectrum obtained with Spitzer/IRS in 2005 March (Figure 1; Ábrahám et al. 2009; Sipos et al. 2009). The two spectra have similar shapes with slight differences. The flux levels are the same at $5 \, \mu m$, but the JWST spectrum has a shallower slope at $5–8 \, \mu m$. Between 8 and $18 \, \mu m$, the two spectra have practically identical shapes, but JWST measured 12% lower flux than Spitzer. Above $18 \, \mu m$, the two spectra again have slightly different slopes: the earlier one is flat, the newer one decreases toward longer wavelengths. We also compared the JWST spectrum with the average of four ISOPHOT/PHOT-S spectra obtained in 1997 February–September (Kóspál et al. 2012) and found that in the overlapping wavelength range ($5.8–11.6 \, \mu m$), they are consistent with MIRI within the uncertainties. These results demonstrate that the MIRI spectrum represents well the quiescent state of EX Lup.

3.2. Dust Features

The characteristic strong, triangular shape of the $10 \, \mu m$ silicate emission feature in the 2005 Spitzer spectrum (Figure 2) was interpreted by Ábrahám et al. (2009) as the signature of amorphous submicron-sized grains. Sipos et al. (2009) fitted this profile and found that the mass fraction of crystalline silicates was <2%. Since the $10 \, \mu m$ feature in our MIRI spectrum has a very similar shape to the Spitzer/IRS, we conclude that the disk of EX Lup contained only small amounts of warm forsterite or enstatite in 2022 August.

In Figure 2 we compared our JWST spectrum with the $10 \, \mu m$ emission profile of amorphous dust grains using the opacity curves of olivine and pyroxene-type silicates. We derived dust opacities using the OPACITYTOOL software (Toon & Ackerman 1981; Min et al. 2005; Woitke et al. 2016),

which is based on the distribution of hollow spheres (DHS) theory (Min et al. 2005). We took the complex refractive index for amorphous silicate from the literature (Dorschner et al. 1995). Following Sipos et al. (2009), we used 0.1 μm-sized olivines and 1.5 μm-sized pyroxenes with a ratio of 2:1. After continuum subtraction, the measured spectral shape can be well reproduced by adopting $T \approx 1200$ K for the underlying blackbody emission, but higher temperatures up to 1500 K give similarly good results.

At longer wavelengths, the MIRI spectrum exhibits several narrower emission peaks at 16.3, 19.0, 20.0, and 23.5 μm. To check if they originate from crystalline silicates, we compared our spectrum with the opacity curves of forsterite grains (Servoin & Piriou 1973). In Figure 2 we plotted the infrared spectrum of small 0.1 μm (green) and larger 2.7 μm (pink) forsterite crystalline grains. We multiplied the opacities by a blackbody curve of 150 K to represent a cold dust population. We found that the small forsterite grains could be responsible for the features peaking around 16.3, 19.0, and 23.5 μm. The additional presence of larger forsterite grains may explain the feature at 20.0 μm.

As our model in Figure 2 shows, small forsterite grains also have an emission peak at 11.3 μm, whose strength depends strongly on the temperature. This feature is not detected in the observed JWST spectrum. Tests with various dust temperatures show that it would be visible for $\geqslant 175$ K. In conclusion, the dust composition in the EX Lup disk is dominated by warm ($T \geqslant 1200$ K) amorphous grains, but a colder ($T \leqslant 150$ K) crystalline silicate, probably forsterite, component is also present.

3.3. Gas Features

The MIRI spectrum of EX Lup also includes a forest of gas emission lines from molecules previously observed in T Tauri disks (Lahuis et al. 2007; Bitner et al. 2008; Carr & Najita 2008, 2011): H_2O, OH, H_2, HCN, C_2H_2, and CO_2. These molecules were identified in EX Lup either during its quiescent phase in 2005 or during its outburst in 2008 using Spitzer/IRS. Line strengths strongly changed between the two epochs, with organics disappearing from the spectrum and stronger OH lines, suggesting effects from UV photodissociation (Banzatti et al. 2012). Additionally, CO rovibrational lines in the fundamental band were previously observed in EX Lup during outburst in 2008 (Goto et al. 2011) and during quiescence in 2014 (Banzatti et al. 2015) using VLT/CRIRES. These data suggested the presence of hot molecular gas in the inner disk during outburst.

The new MIRI data show the 4.9–27 μm mid-infrared spectrum of EX Lup for the first time since 2008, covering all of the above-mentioned molecular lines at high resolution, allowing us to study longer-term chemical changes induced by an accretion outburst. In this first paper, we only provide a brief overview of the most prominent lines observed in the spectrum and illustrate the approximate match to slab models. The in-depth analysis of the molecular emission is left to an upcoming paper.

For line identification, we produced synthetic spectra using a slab model in local thermodynamic equilibrium following Banzatti et al. (2012), with molecular data from the latest HITRAN release (Gordon et al. 2022). We adopted parameters from previous works and adjusted them by eye to match the relative strength of gas emission lines in the MIRI data.

Figure 3 displays portions of the continuum-subtracted spectrum showing all the major molecules observed. Hundreds of H_2O lines are detected from rovibrational bands below 8 μm and from pure rotational transitions between 12 and 28 μm. Compared to previous Spitzer spectra, most of these lines are now deblended in the MIRI spectrum, with some blending still visible at the shortest wavelengths. In Figure 3, we show two slab models for water using properties previously found from fits to high-resolution ground-based spectra of other T Tauri disks (Banzatti et al. 2023): $T \sim 1000$ K for the rovibrational lines below 6.6 μm and $T \sim 600$ K for the rotational lines at 13–16 μm, and a similar column density of $\approx 10^{17}$–10^{18} cm^{-2}.

For CO we adopted properties found previously in high-resolution spectra that covered lines up to $J = 50$ (Banzatti et al. 2022): $T \sim 800$ K and $N_{CO} \sim 10^{19}$ cm^{-2}. Since MIRI has insufficient resolution to distinguish the broad (BC) and narrow (NC) velocity components observed in ground-based data, we adopted here T and N in between those estimated for BC and NC in other disks (see Figure 11 in Banzatti et al. 2022). The relative weakness of the $v = 2 - 1$ lines suggests subthermal vibrational excitation, so we used a lower vibrational temperature $T_{vib} \sim 450$ K.

Detection of rovibrational emission from C_2H_2, HCN, and CO_2 demonstrates that the organic molecules are back after disappearing during the 2008 outburst. The Q-branch emission lines (near 13.7 μm, 14.0 μm, and 14.9 μm respectively) are still blended at the resolution of MIRI, but several weak lines are now detected for the first time from the P and R branches. For HCN, multiple peaks in the Q branch are distinguished with MIRI. The slab models in Figure 3 assumed $T \sim 300$–800 K and column density of $\approx 10^{15}$–10^{16} cm^{-2} as found from previous analyses of Spitzer spectra of T Tauri disks (Carr & Najita 2011; Salyk et al. 2011).

Multiple weak lines from OH are detected throughout the spectrum. Mid-infrared OH emission has previously shown very high temperatures indicative of production from UV photodissociation of water (Carr & Najita 2014) and was found to increase during the 2008 outburst in EX Lup (Banzatti et al. 2012). In Figure 3, we use $T \sim 4000$ K and $N \sim 10^{16}$ cm^{-2}.

Several rotational lines of molecular hydrogen (H_2) are detected from 0–0 S(8) at 5.05 μm to 0–0 S(1) at 17.03 μm (Roueff et al. 2019). Some of the lines are blended with CO or H_2O, but S(1), S(3), S(4), S(5), and S(7) are well resolved.

Lines of longer-chain hydrocarbons (C_2H_4 at 10.5 μm) or aromatic hydrocarbons (benzene, C_6H_6, at 5.1 and 5.5 μm) were not found. We also searched for CH_3OH (9.7 μm), CH_4 (7.6 μm), NH_3 (10.1–10.9 μm), and H_2CO (5.7 μm), but found no such lines in the MIRI spectrum of EX Lup at this stage of the data reduction and analysis.

4. Discussion

4.1. Quiescent Disk Variability

In quiescence, EXors have accretion rates similar to regular T Tauri stars (Lorenzetti et al. 2012); therefore, their disks should also be similar to those of normal T Tauri disks. Indeed, the MIRI spectrum of EX Lup is similar to typical T Tauri disk spectra (e.g., Furlan et al. 2006; Kessler-Silacci et al. 2006). Sipos et al. (2009) studied the quiescent spectral energy distribution (SED) of EX Lup and found that its shape is very similar to the median SED of T Tauri stars in the Taurus star-forming region. Interestingly, their radiative transfer modeling
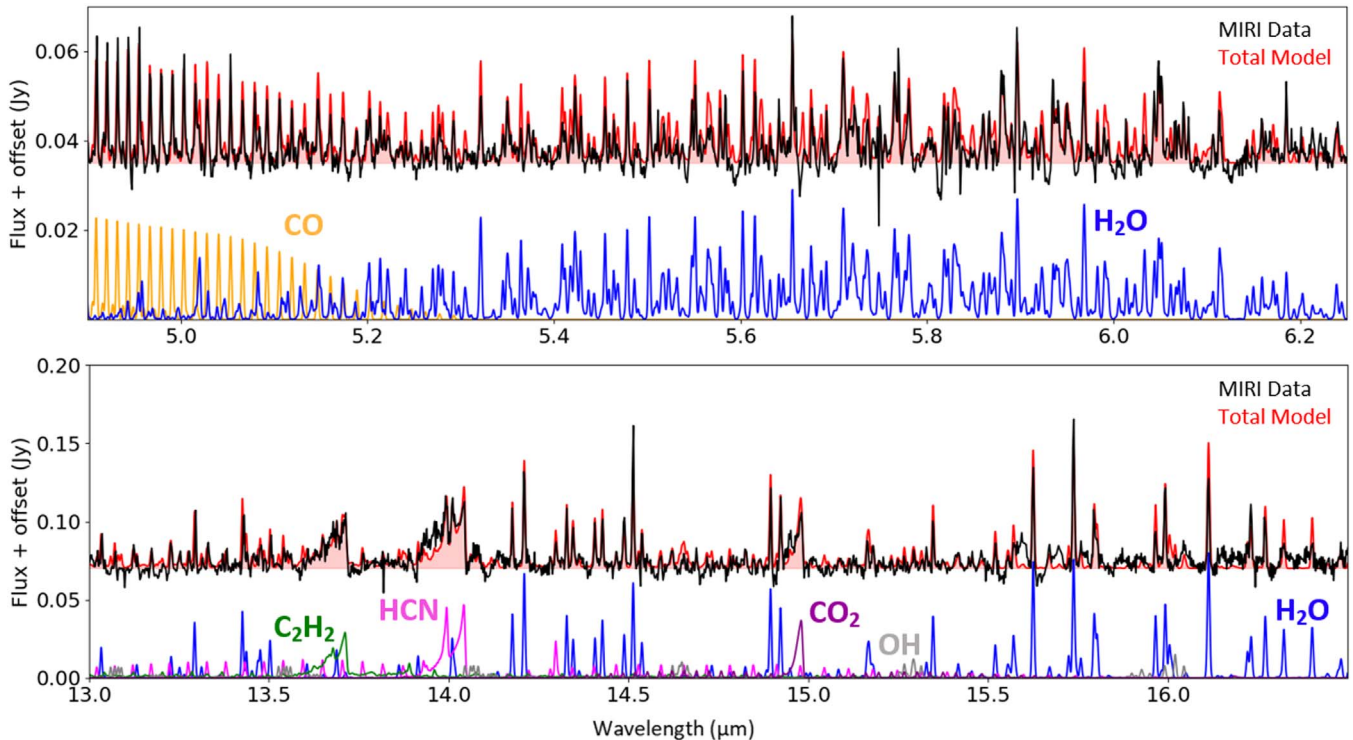
Figure 3. Continuum-subtracted MIRI spectrum with slab models for the identification of molecular lines.

revealed that the dust disk of EX Lup does not extend inward until the dust sublimation radius (0.06 au), but it has a larger inner radius at about 0.2–0.3 au.

While the general shape of the 5–27 μm spectrum of EX Lup is very similar between 2005 (Spitzer) and 2022 (JWST), the object was somewhat (<25%) fainter in 2022. Such small infrared variability is not unusual for EX Lup in quiescence, because multiple quiescent Spitzer spectra (2004 August, 2005 March, and 2009 April) also show differences up to 20%. A comparison of Spitzer and ISO spectra of EX Lup by Kóspál et al. (2012) also revealed only minor changes.

Interestingly, the slope of the SED in the 5–8 μm and 24–27 μm ranges as measured by JWST is different from those in 2005. Such variations of the infrared spectral slope, and in certain cases, anticorrelation between shorter and longer mid-infrared wavelengths with a pivot point in between was noticed in other young stars and has been explained with variable inner rim height and variable shadowing of the outer disk (Muzerolle et al. 2009; Espaillat et al. 2011; Flaherty et al. 2011; Kóspál et al. 2012). In EX Lup, the shallower slope at shorter wavelengths may indicate more warm material or a larger scale height around the inner edge of the dust disk. The radius of the inner edge might also have changed between the two epochs. The decreasing slope at longer wavelengths as opposed to the earlier flat SED may point to the possibility that the outer part of the disk received less illumination in 2022 than in 2005.

4.2. Silicate Crystals toward the Snowline

In Section 3.2 we showed that the profile of the 10 μm silicate feature in our JWST spectrum is very similar to that observed with Spitzer/IRS in 2005, prior to the large outburst. Thus, JWST confirmed that the crystalline forsterite grains, produced in 2008 through thermal annealing on the disk surface between 0.3 and 0.7 au and detected via their 10 and

11.3 μm emission by Ábrahám et al. (2009, 2019), are no longer present in the inner disk. This result is consistent with VLTI/MIDI data from 2013 and VLT/VISIR data from 2016, which also failed to detect the crystalline features at 10 and 11.3 μm, although at a lower significance level (Ábrahám et al. 2019).

The hypothesis of Juhász et al. (2012) and Ábrahám et al. (2019), that the forsterite grains formed in 2008 still exist but were transported to outer colder disk regions (Section 1), could not be verified after the end of the cryogenic mission of Spitzer (2009 May) until now. The unambiguous detection of cold crystalline features in the 16–26 μm range of the JWST/MIRI spectrum, however, implies that we very likely rediscovered the forsterite grains that were inaccessible for the available instrumentation for more than a decade.

To infer the radial location of the cold crystals, we compared the measured crystalline profiles with synthetic spectra computed by Ábrahám et al. (2019) for a model containing a disk made of amorphous dust grains and an expanding hollow sphere made of crystalline forsterite, assuming three different radii for the sphere: 3 au, 5 au, and 9.68 au. Figure 4 presents this comparison. The strength of the 23.5 μm band suggests that our JWST measurement is most consistent with a radial distance of ~3 au for the current location of the crystalline material.

The derived radial distance of ~3 au suggests that the crystalline grains formed in 2008 may now be in the vicinity of the water snowline: a disk region where the temperature drops to 150–170 K and water molecules freeze out onto grain surfaces (at 3.5 au on the surface of EX Lup's disk). The temperature of ⩽150 K, estimated for the crystalline dust in Section 3.2, is fully consistent with this conclusion. We have very limited information on the spatial distribution of the crystals. Their geometry is probably determined by the
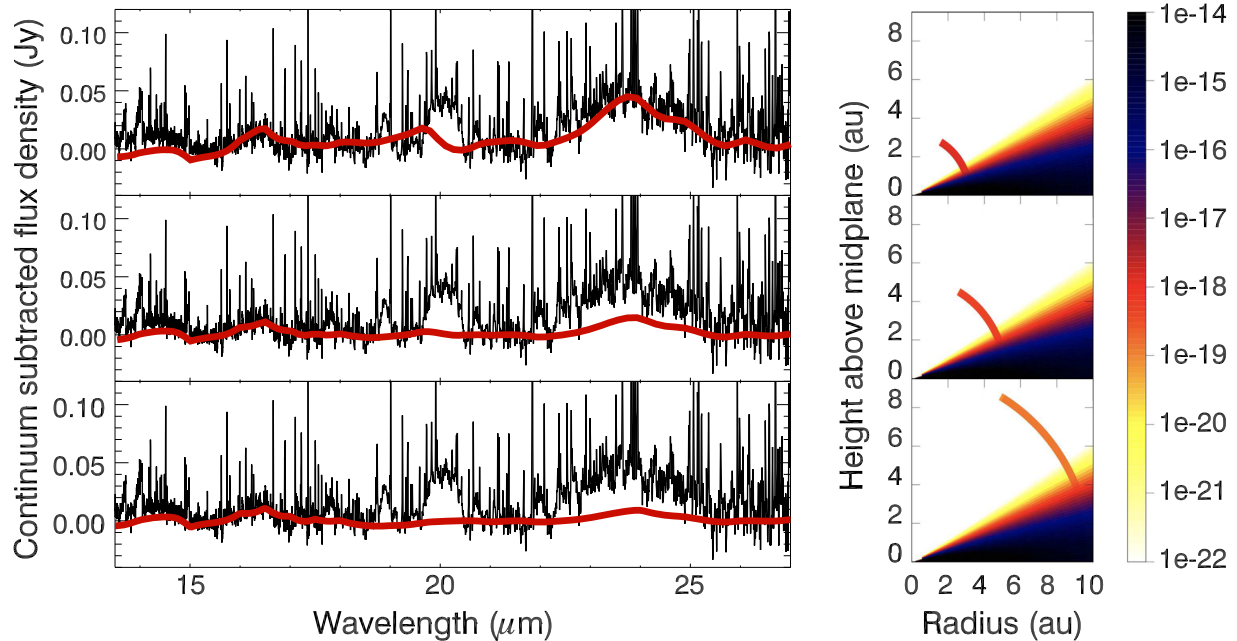
Figure 4. Left: continuum-subtracted JWST/MIRI spectrum of EX Lup (black) and model spectra including an amorphous disk and a hollow crystalline sphere placed at different radii (red). Right: density distributions of the various models (in g cm^{-3}). Models are from Figure 2 of Ábrahám et al. (2019).

properties of the wind that provides the momentum for the transportation of the grains.

Ábrahám et al. (2019) proposed that the crystals were at 3 au already in 2013. As the current JWST spectrum indicates that the crystalline grains are still at 3 au, their radial expansion might have slowed down. Thus, they are not expected to move significantly farther away from the star in the future. However, they may not stay undisturbed in their current location either. In 1955/56, EX Lup underwent a large outburst, similar to the one in 2008 (Herbig 1977), and it is reasonable to assume that a comparable amount of crystalline silicates was then produced. Those grains could have also moved outward, but the Spitzer spectrum in 2005 exhibited no cold forsterite emission (Figure 2), suggesting that something happened with the cooled-down crystalline grains on decadal timescales.

Vertical mixing in the disk could remove the crystals from the surface. Figure 6 in the Supplementary Material of Ábrahám et al. (2009) shows that at a radial distance of 3 au, a turbulent viscosity parameter α of a few times 10^{-2} gives a vertical mixing timescale of $\leqslant 50$ yr. Alternatively, crystalline particles may start growing ice mantles as they move outward, leading to the nondetection of well-defined mid-infrared spectral features due to the increased grain size. Using Equation (12) from Rab et al. (2017) and adopting representative parameters for the EX Lup disk at 3 au close to the vertical water ice line, we obtain a freeze-out timescale of about 3 yr. Based on these considerations, we anticipate changes in the strength of the crystalline spectral features during the next years/decades in EX Lup. Future monitoring with JWST will be invaluable to follow this evolution.

When the crystalline grains reach the snowline, they may acquire ice mantles, and the increased collisional cross section and stickiness would facilitate future incorporation into planetesimals, including icy protocomets. If all the crystalline grains produced in the 2008 outburst end up in the water snowline region, that would add $\sim 1.9 \times 10^{23}$ g (equal to 10^4 times the mass of comet Hale–Bopp) to the crystalline dust

reservoir (Ábrahám et al. 2019). If similar large outbursts occur every 50 yr for an extended period of 10^5 yr, the total yield would be $2 \times 10^{-7} M_\odot$. Based on these numbers, we propose that large eruptions of young stars may be a significant source of crystalline grains in planetesimals and ultimately in the planet-building material.

4.3. Future Prospects

The MIRI spectrum in 2022 provides the first opportunity to study mid-infrared molecular lines since the 2008 outburst. The organic molecules that disappeared in 2008 have now been detected again. Modeling of these (and other) lines in the JWST spectrum and a detailed study of their time variability will be the topic of a future paper. The increased spectral resolution of JWST/MIRI MRS (as compared to Spitzer/IRS) and the high S/N of the spectrum will allow us to deblend and fit the various molecules, providing more stringent constraints than ever before on the thermal structure and molecular abundances in EX Lup's disk. We demonstrated that the spectrum also provides unprecedentedly rich information on various silicate components and their temperature distribution, allowing the characterization of the planet and comet-forming solids. Reobserving EX Lup with the JWST will provide a unique opportunity to monitor long-term chemical and mineralogical changes in the disk due to variable accretion.

ORCID iDs

Ágnes Kóspál ⬤ https://orcid.org/0000-0001-7157-6275
Péter Ábrahám ⬤ https://orcid.org/0000-0001-6015-646X
Andrea Banzatti ⬤ https://orcid.org/0000-0003-4335-0900
Jeroen Bouwman ⬤ https://orcid.org/0000-0003-4757-2500
Lei Chen ⬤ https://orcid.org/0000-0003-2835-1729
Fernando Cruz-Sáenz de Miera ⬤ https://orcid.org/0000-0002-4283-2185
Joel D. Green ⬤ https://orcid.org/0000-0003-1665-5709
Thomas Henning ⬤ https://orcid.org/0000-0002-1493-300X
Christian Rab ⬤ https://orcid.org/0000-0003-1817-6576

References

Ábrahám, P., Chen, L., Kóspál, Á., et al. 2019, ApJ, 887, 156
Ábrahám, P., Juhász, A., Dullemond, C. P., et al. 2009, Natur, 459, 224
Banzatti, A., Abernathy, K. M., Brittain, S., et al. 2022, AJ, 163, 174
Banzatti, A., Meyer, M. R., Bruderer, S., et al. 2012, ApJ, 745, 90
Banzatti, A., Pontoppidan, K. M., Bruderer, S., Muzerolle, J., & Meyer, M. R. 2015, ApJL, 798, L16
Banzatti, A., Pontoppidan, K. M., Pérez Chávez, J., et al. 2023, AJ, 165, 72
Bitner, M. A., Richter, M. J., Lacy, J. H., et al. 2008, ApJ, 688, 1326
Boogert, A. C. A., Pontoppidan, K. M., Knez, C., et al. 2008, ApJ, 678, 985
Carr, J. S., & Najita, J. R. 2008, Sci, 319, 1504
Carr, J. S., & Najita, J. R. 2011, ApJ, 733, 102
Carr, J. S., & Najita, J. R. 2014, ApJ, 788, 66
Cieza, L. A., Casassus, S., Tobin, J., et al. 2016, Natur, 535, 258
Dent, W. R. F., Thi, W. F., Kamp, I., et al. 2013, PASP, 125, 477
Dorschner, J., Begemann, B., Henning, T., Jaeger, C., & Mutschke, H. 1995, A&A, 300, 503
Eistrup, C., & Henning, T. 2022, A&A, 667, A160
Espaillat, C., Furlan, E., D'Alessio, P., et al. 2011, ApJ, 728, 49
Fabian, D., Henning, T., Jäger, C., et al. 2001, A&A, 378, 228
Fedele, D., Bruderer, S., van Dishoeck, E. F., et al. 2013, A&A, 559, A77
Fischer, W. J., Hillenbrand, L. A., Herczeg, G. J., et al. 2022, arXiv:2203.11257
Flaherty, K. M., Muzerolle, J., Rieke, G., et al. 2011, ApJ, 732, 83
Furlan, E., Hartmann, L., Calvet, N., et al. 2006, ApJS, 165, 568
Gordon, I. E., Rothman, L. S., Hargreaves, R. J., et al. 2022, JQSRT, 277, 107949
Goto, M., Regály, Z., Dullemond, C. P., et al. 2011, ApJ, 728, 5
Henning, T. 2010, ARA&A, 48, 21
Herbig, G. H. 1977, ApJ, 217, 693
Herbig, G. H. 1989, in ESO Conf. and Workshop Proc. 33, ESO Workshop on Low Mass Star Formation and Pre-main Sequence Objects, ed. B. Reipurth (Garching: European Southern Observatory), 233
Jørgensen, J. K., Belloche, A., & Garrod, R. T. 2020, ARA&A, 58, 727
Juhász, A., Dullemond, C. P., van Boekel, R., et al. 2012, ApJ, 744, 118
Kessler-Silacci, J., Augereau, J.-C., Dullemond, C. P., et al. 2006, ApJ, 639, 275
Kester, D. J. M., Beintema, D. A., & Lutz, D. 2003, in The Calibration Legacy of the ISO Mission, ESA SP-481, ed. L. Metcalfe et al. (Noordwijk: ESA), 375
Kóspál, Á., Ábrahám, P., Acosta-Pulido, J. A., et al. 2012, ApJS, 201, 11
Kóspál, Á., Fiorellino, E., Ábrahám, P., Giannini, T., & Nisini, B. 2022, RNAAS, 6, 52
Lahuis, F., van Dishoeck, E. F., Blake, G. A., et al. 2007, ApJ, 665, 492
Lorenzetti, D., Antoniucci, S., Giannini, T., et al. 2012, ApJ, 749, 188
Min, M., Hovenier, J. W., & de Koter, A. 2005, A&A, 432, 909
Molyarova, T., Akimkin, V., Semenov, D., et al. 2018, ApJ, 866, 46
Muzerolle, J., Flaherty, K., Balog, Z., et al. 2009, ApJL, 704, L15
Pontoppidan, K. M., Salyk, C., Blake, G. A., et al. 2010, ApJ, 720, 887
Rab, C., Elbakyan, V., Vorobyov, E., et al. 2017, A&A, 604, A15
Roueff, E., Abgrall, H., Czachorowski, P., et al. 2019, A&A, 630, A58
Salyk, C., Pontoppidan, K. M., Blake, G. A., Najita, J. R., & Carr, J. S. 2011, ApJ, 731, 130
Servoin, J. L., & Piriou, B. 1973, PSSBR, 55, 677
Sipos, N., Ábrahám, P., Acosta-Pulido, J., et al. 2009, A&A, 507, 881
Toon, O. B., & Ackerman, T. P. 1981, ApOpt, 20, 3657
van Dishoeck, E. F. 2004, ARA&A, 42, 119
Williams, J. P., & Cieza, L. A. 2011, ARA&A, 49, 67
Woitke, P., Min, M., Pinte, C., et al. 2016, A&A, 586, A103
Wordsworth, R., & Kreidberg, L. 2022, ARA&A, 60, 159
Zhou, L., & Herczeg, G. J. 2022, ATel, 15271, 1